PFC/JA-87-46

# Quasi-Optical Gyrotron With Arbitrary Beam Injection Angle

Wang*, C.Y.; Kreischer, K.E.; Temkin, R.T.

November 1987

Plasma Fusion Center
Massachusetts Institute of Technology
Cambridge, MA 02139

*Visiting scientist from Zhejiang Univ., Hangzhou, P.R. China

December 11, 1987

# Quasi-Optical Gyrotron With Arbitrary Beam Injection Angle

C. Y. Wang *  K. E. Kreischer
R. J. Temkin
Massachusetts Institute of Technology
Plasma Fusion Center
Cambridge, MA 02139

In quasi-optical gyrotrons the beam injection angle (angle between the electron beam and radiation beam) has considerable influence on the gain, harmonic operation and efficiency. This paper investigates the effect on the gain mechanism. Two regimes of operation are identified, namely gain nearly proportional to $l^2$ ($l$ is the interaction length) for small angles and gain nearly proportional to $l^3$ for large angles. The transition angle separating the two regimes is found and is approximately given by $(\lambda/l)^{1/2}$ where $\lambda$ is the wave length. By choosing the parameters appropriately one can run the gyrotron in the high gain regime.

*Visiting scientist from Zhejiang Univ., Hangzhou, P. R. China

# 1. Introduction

Great progress made in controlled nuclear fusion research has resulted in new demands for gyrotrons with higher performances for tokamak plasma heating. Research efforts are being made at many laboratories to pursue higher frequencies and greater powers. To circumvent the serious problem of mode competition encountered in high-frequency gyrotrons, quasi-optical cavities[1-6,9-13] have been adopted as one of the approaches. In the past, most of theoretical and experimental work has dealt with cases where the radiation and electron beams are in either parallel or perpendicular configurations. Ref.[1] to [6] have analyzed geometries with an arbitrary beam injection angle. However the influence of the angle on the interaction mechanism has not been fully explored so far.

Analysis shows that the angle between radiation and electron beams influences gain, harmonic performance and efficiency. It adds both flexibility and complication to gyrotron performance. This paper will dwell on the topic of gain mechanisms. In Section 2 the general gain mechanism in quasi-optical gyrotrons is analyzed. In Section 3 the influences of various angles on the gain mechanisms are investigated. Section 4 gives conclusions.

# 2. General Analysis of the Quasi-optical Gyrotron Gain

From Ref. [2] the linear efficiency can be formulated as

$$\eta = \frac{E_0^2 e^2 G}{8\gamma(\gamma-1)m^2c^2v_{\|}^2} \tag{1}$$

where $E_0$ is the amplitude of the electric field, $v_{\|}$ is the velocity component of the electron parallel to the d-c magnetic field, $\gamma$ is the relativistic energy factor of the electron, c is the light velocity, e and m are the electric charge and the mass of the electron respectively. The gain function G is

$$G = l^3 k \frac{\beta_\perp^2}{\beta_{\|}} \frac{d\tilde{F}_1}{dx}(1 - x^2 cos^2\theta) - l^2 \left[ \left( 2\beta_{\|} + \frac{2\beta_\perp^2}{\beta_{\|}} \right) x\tilde{F}_1 cos\theta + 2\tilde{F}_1 \right] \tag{2}$$

where

$$\tilde{F}_1 = \frac{1}{(1-x)^2}\frac{1-cos\xi}{\xi^2} \tag{3}$$

$$\frac{d\tilde{F}_1}{dx} = \frac{4x}{(1-x)^3}\frac{(1-cos\xi)}{\xi^3} + \frac{1}{(1-x)^2}\frac{sin\xi}{\xi^2} \tag{4}$$

detuning $\xi = q\pi(1+x), x = (\omega_c - \omega)/(k_{\|}v_{\|}), k_{\|} = kcos\theta, \omega_c = eB_0/(\gamma mc)$, q is the number of standing wave peaks within the interaction length, $\omega$ and k are the circular frequency and wave number of the plane wave, $\theta$ is the angle between the radiation and electron beams and $l$ is the interaction length. In this paper we only discuss the uniform field profile.

As pointed out in Ref.[2], the first two terms in Eq. (2) result from the relativistic dependence of the electron cyclotron frequency on velocity. The first term is caused by interaction of electrons with electric fields and contributes mainly in the ECRM instability. The second term comes from axial bunching caused by $\mathbf{v}_\perp \times \mathbf{B_1}$ ($\mathbf{B_1}$ is the magnetic field of the electromagntic wave) force which also produces the fourth term. These two terms correspond to the Weibel instability. The third term comes from transverse bunching caused by $\mathbf{v}_{\|} \times \mathbf{B_1}$. The last term results from energy absorption.

One can see from Eqs. (2) and (4) that the first two terms scale as $l^3$ and can be much bigger than the other three terms. They always counteract each other, which is a unique characteristic for gyrotron interaction[7]. This situation determines two operation regimes for the quasi-optical gyrotron with arbitrary beam injection angle.

In the first regime, which occurs for larger angles, the first term dominates in Eq.(2). In this case the gain scales as $l^3$. Plotting the first term versus $\xi$ in Fig.1a one can see that it reaches its maximum at approximately

$$\xi_1 = -2.5 \tag{5}$$

When the maximum of the total gain is reached at $\xi = -2.5$, we define it the $l^3$ gain regime. In this regime, the gain scales as length to a power that is nearly equal to 3. The exact gain scaling as a function of angle will be discussed below. Note that the gain characteristics are the same as those for the free electron laser[8].

In the second regime, which occurs at small angles, the first two terms are comparable but still remain much bigger than the remaining three terms. When $\theta = 0$, one can see that the first two terms scale as $l^2$ since $1 - x^2 = (1 - x)\xi/q\pi \approx 2\xi/k_{\|}l$. A plot of the first two terms is given in Fig.1b. The main maximum is reached at about

$$\xi_2 = 7.5 \tag{6}$$

When the maximum of the total gain is reached at $\xi = 7.5$, we define it the $l^2$ gain regime. The minor maximum is reached at about $\xi = -7.5$. These also correspond to the maximum points of the $l^2$ gain regime.

## 3. Influence of Injection Angle on Gain Mechanism

Since the theory in Ref.1 is a one-dimensional model while with a nonzero injection angle the finite size of the radiation beam cross-section must be taken into account, a finite optical beam radius, $w$, is imposed on the calculation model (see Fig.2). A plane wave model was used for the optical mode inside the resonator.

Define an angle

$$\theta_0 = arctan\left(\frac{2w}{L}\right) \tag{7}$$

The interaction length is determined according to

$$l = \begin{cases} L/cos\theta & \text{if } \theta \leq \theta_0 \\ 2w/sin\theta & \text{if } \theta \geq \theta_0 \end{cases} \tag{8}$$

Note that this definition of $l$ is important in providing correct limiting values as $\theta$ approaches $90^0$. The conclusions presented in this paper are not dependent on the specific value of $\theta_0$ in Eq.7.

The gain (Eq.2) has been calculated versus detuning $\xi$ for various angles with f=140GHz, V=50kv, $v_{\perp}/v_{\|}$=2 and q=46 corresponding to a cavity length of 4.9cm. The curves are shown in Fig.3. One can see that when $\theta = 0$ the gain spectrum is nearly symmetrical with two maxima, the one near $\xi = 7.5$ being slightly higher. Tilting the beam a little the spectrum becomes asymmetrical, the minor maximum shifting toward $\xi$ = -2.5 while

the main maximum remains the same, which can be seen from Fig.3b and Fig.3c. When $\theta > 12^0$, the main maximum begins to drop and the highest gain is reached near $\xi$ = -2.5, which is shown in Fig.3d and Fig.3e. When $\theta > 24^0$, the spectrum remains nearly antisymmetrical as is shown in Fig.3f.

A plot of $\xi$ at maximum gain versus angle is shown in Fig.4. One can see there exist two distinct operation regimes, one in $\theta < 12^0$, the other in $\theta > 24^0$. These are the very $l^2$ and $l^3$ gain regimes described in §2. Between these regimes is a transition region.

A plot of maximum gain versus angle is shown in Fig.5. One can see a dramatic rise in gain when $\theta$ increases from $12^0$ to above $24^0$.

A plot of the first, last and remaining terms of Eq.2 is shown in Fig.6. The top curve corresponds to contributions from the electric fields, the middle from absorption and the bottom from $\mathbf{v} \times \mathbf{B_1}$ force. One can see that at $\theta = 12^0$ both gains due to $\mathbf{E_1}$ and $\mathbf{B_1}$ fields rise dramatically but in opposite direction. After reaching maxima simultaneously, they both drop down. At $\theta = 90^0$ the $\mathbf{B_1}$ field gain vanishes and only the $\mathbf{E_1}$ gain remains. This is because when the wave vector $\mathbf{k}$ is perpendicular to z axis, the $\mathbf{B_1}$ field will be parallel to z axis so that $\mathbf{v} \times \mathbf{B_1} = \mathbf{v}_\perp \times \mathbf{B_1}$. In the integral for the perturbed distribution function the $\mathbf{B_1}$ field contribution

$$(\mathbf{v} \times \mathbf{B_1}) \cdot \frac{\partial f_0}{\partial \mathbf{p}} = (\mathbf{v}_\perp \times \mathbf{B_1}) \cdot (\frac{\partial f_0}{\partial \mathbf{p}_\perp} + \frac{\partial f_0}{\partial \mathbf{p}_\parallel}) \tag{9}$$

and $(\mathbf{v}_\perp \times \mathbf{B_1}) \cdot (\partial f_0 / \partial \mathbf{p}_\perp) \equiv \mathbf{0}$ and $(\mathbf{v}_\perp \times \mathbf{B_1}) \cdot (\partial f_0 / \partial \mathbf{p}_\parallel) \equiv \mathbf{0}$ since $\mathbf{B_1} \parallel \mathbf{p}_\parallel$.

The influence of the absorption term is small. Fig.7 gives contributions from the second term (lower curve) and the third and fourth terms (upper curve) of Eq.2. Fig.8 gives the log gain versus log cavity length under various angles. One can see the obviously different scalings between regions $\theta \leq 10^0$ and $\theta > 10^0$. These are the very $l^2$ and $l^3$ gain regimes.

To define the transition from the $l^2$ regime to $l^3$ regime, one can determine the transition angle at which the gain calculated with $\xi = \xi_1$ equals the gain calculated with $\xi = \xi_2$. This results in the following equation:

$$\left\{ \frac{\beta_\perp^2}{\beta_\parallel} \left[ \frac{2}{3} x_1^2 F_2(\xi_1) - x_2^2 F_2(\xi_2) \right] + 2 \left( \beta_\parallel + \frac{\beta_\perp^2}{\beta_\parallel} \right) \left[ x_1 F_1(\xi_1) - x_2 F_1(\xi_2) \right] \right\} cos^2\theta$$

$$+2[F_1(\xi_1) - F_1(\xi_2)]cos\theta + \frac{\beta_\perp^2}{\beta_\parallel}\left[F_2(\xi_2) - \frac{2}{3}F_2(\xi_1)\right] = 0 \quad (10)$$

where

$$F_1(\xi) = \left(\frac{q\pi}{1-x}\right)^2 \frac{(1-cos\xi)}{2\xi^2} \quad (11)$$

and

$$F_2(\xi) = \frac{(q\pi)^3}{8}\left(\frac{\xi cos\xi - sin\xi}{\xi^2}\right) \quad (12)$$

$\xi_1$ and $\xi_2$ are the detunings corresponding to the maxima in the regions $\xi < 0$ and $\xi > 0$ respectively. Note that in the transition region $\xi_1 \neq -2.5$ as in Eq.5. The maximum must be searched for in the region $\xi < 0$. Since $\xi$ is a function of $cos\theta$, Eq.10 must be solved by iteration.

A plot of the transition angle versus interaction length for two groups of quite diverse parameters is given in Fig.9. The horizontal lines indicate there is no solution for Eq.10. One can see that the transition angle does not change drastically with different cases and they range roughly from $5^0$ to $12^0$. This is due to the fact that in the transition region $\xi_2$ remains unchanged at 7.5 and the coefficients of Eq.10 change nearly proportionally. So the transition angle is not sensitive to the change of parameters.

An approximate expression for the transition angle can be obtained by neglecting the $l^2$ terms in Eq.2 and approximating $cos\theta$ with $1 - \theta^2/2$. One can show that the gain is proportional to

$$l^3\frac{d\tilde{F}_1(\xi)}{d\xi}[\xi - \xi\theta^2/2 + \pi(l/\lambda)\theta^2] \approx l^3\frac{d\tilde{F}_1(\xi)}{d\xi}[\xi + \pi(l/\lambda)\theta^2] \quad (13)$$

if $\xi \ll 2\pi(l/\lambda)$, which is often the case. The maximum of this function changes from $\xi \simeq 7.5$ to $\xi \simeq -2.5$ when $\pi(l/\lambda)\theta^2 \simeq 3.4$. Thus one can write

$$\theta_{trans}^2 \simeq \lambda/l \quad (14)$$

This is in agreement with the results of Fig.8 and 9. In particular, Eq.14 predicts the transition from $l^2$ to $l^3$ gain in the $20^0$ case of Fig.8. In fact, $\theta_{trans}$ will depend weakly on the beam parameters due to the effect of the $l^2$ terms.

## 4. Conclusion

Influence of beam injection angles on the operation mechanism of quasi-optical gyrotron is investigated in this paper. Analysis shows that there are two regimes of operation separated by a transition angle. Above the transition angle is the $l^3$ gain regime where the azimuthal bunching term caused by the $\mathbf{E_1}$ field dominates the opposing main Weibel term. Below the transition angle is the $l^2$ gain regime where these two terms nearly cancel. By choosing parameters appropriately one can run the quasi-optical gyrotron in the $l^3$ high gain regime.

## 5. Acknowledgements

The authors would like to thank Dr. C.M.Tang for useful discussions. This research was conducted under U.S.D.O.E. contract DE-AC02-78ET-51013.

## References


[1] V.L.Bratman, N.S.Ginzburg, G.S.Nusinovich, M.I.Petelin and P.S.Strelkov, Int.J.Electronics, Vol.51,No.4,541(1981)

[2] K.E.Kreischer and R.J.Temkin, *Infrared and Millimeter Waves*, Vol.7, Chap.8, Academic Press. Inc. 377(1983)

[3] S.Liu, *Acta Electronica Sinica*, Vol.12,No.1,12(1984)

[4] P.Sprangle, C.M.Tang and P.Serafim, Nucl. Instr. & Methods in Phys. Research, A250,361(1986)

[5] C.M.Tang, S.Riyopoulos, P.Sprangle and B.Levush, NRL Mem.Rpt. 5947(1987)

[6] A.Gover, A.Friedman, G.Kurizki, S.Ruschin and A.Yariv, submitted for publication

[7] K.R.Chu and J.L.Hirshfield, Phys.Fluids,Vol.21,No.3,461(1978)

[8] W.B.Colson, Phys.Lett.59A,187(1976)

[9] F.A.Korolev and A.F.Kurin, Radio Eng. Electron Phys.(USSR),Vol.15, 1868(1970)

[10] J.L.Vomvoridis, P.Sprangle and W.M.Manheimer, *Infrared and Millimeter Waves*, Vol.7, Chap.9, Academic Press. Inc. 487(1983)

[11] A.Bondeson, W.M.Manheimer and E.Ott, ibid., Vol.9,Chap.7,309 (1983)

[12] T.A.Hargreaves, K.J.Kim, J.H.McAdoo, S.Y.Park, R.D.Seeley and M.E.Read, Int.J.Electronics, Vol.57,No.6,977(1984)

[13] M.Q.Tran, A.Bondeson, A.Perrenoud, S.Alberti, B.Isaak and P.Muggli, ibid.,Vol.61,No.6,1029(1986)


FIGURE CAPTIONS

- Fig.1a Sample spectrum for $l^3$ gain.

- Fig.1b Sample spectrum for $l^2$ gain.
- Fig.2 A model for calculation. l is the interaction length, L is the cavity length, w is the mirror radius, $\theta$ is the angle between radiation beam and electron beam.
- Fig.3a Gain from Eq.(2) is plotted vs. detuning $\xi$ at $0^0$ for a 50kV electron beam, $\alpha$=2, f=140GHz, number of half-wavelengths = 46, cavity length = 4.92857cm, mirror radius = 0.58cm.
- Fig.3b Gain spectrum for $5^0$. The parameters are the same as Fig.3a.
- Fig.3c Gain spectrum for $12^0$. The parameters are the same as Fig.3a. This is a critical case, after which the gain scales as $l^3$.
- Fig.3d Gain spectrum for $14^0$. The parameters are the same as Fig.3a.
- Fig.3e Gain spectrum for $24^0$. The parameters are the same as Fig.3a.
- Fig.3f Gain spectrum for $60^0$. The parameters are the same as Fig.3a.
- Fig.4 Detuning at the maximum gain versus various angles. The parameters are the same as Fig.3a.
- Fig.5 Maximum gain versus angle. The parameters are the same as Fig.3a.
- Fig.6 Contributions from various gain terms in Eq.(2). The parameters are the same as Fig.3a. The upper line is the contribution from the electric field. The middle line is that from absorption. The lower line is that from the magnetic field.
- Fig.7 Contributions from V cross B terms. The parameters are the same as Fig.3a. The upper line is from $l^2$ terms while the lower line is from the $l^3$ term.
- Fig.8 Log of maximum gain versus log of interaction length at different angles. Frequency = 140.GHz, voltage = 50kV, velocity ratio = 2.0, interaction length varies from 1cm to 5cm.

- Fig.9a Transition angle versus number of standing wave peaks within the interaction length. Frequency = 140GHz, voltage = 50kV, velocity ratio = 2.0.

- Fig.9b Transition angle versus number of standing wave peaks within the interaction length. Frequency = 280GHz, voltage = 700kV, velocity ratio = 0.6.

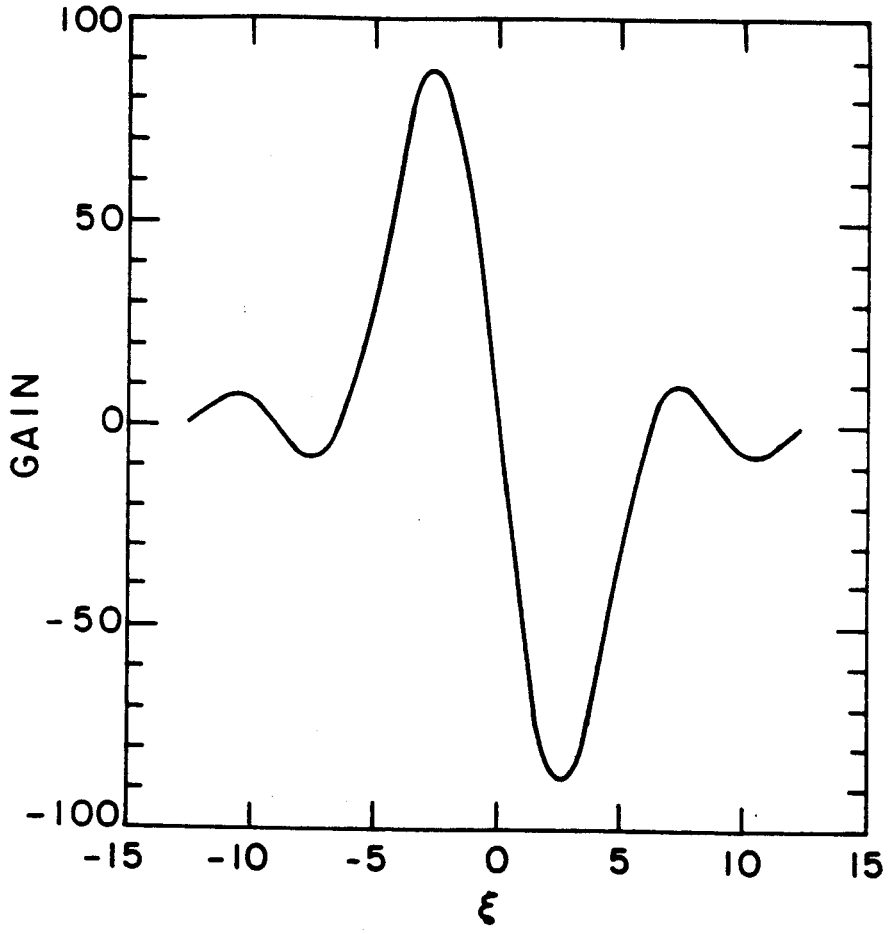


Fig. 1.a

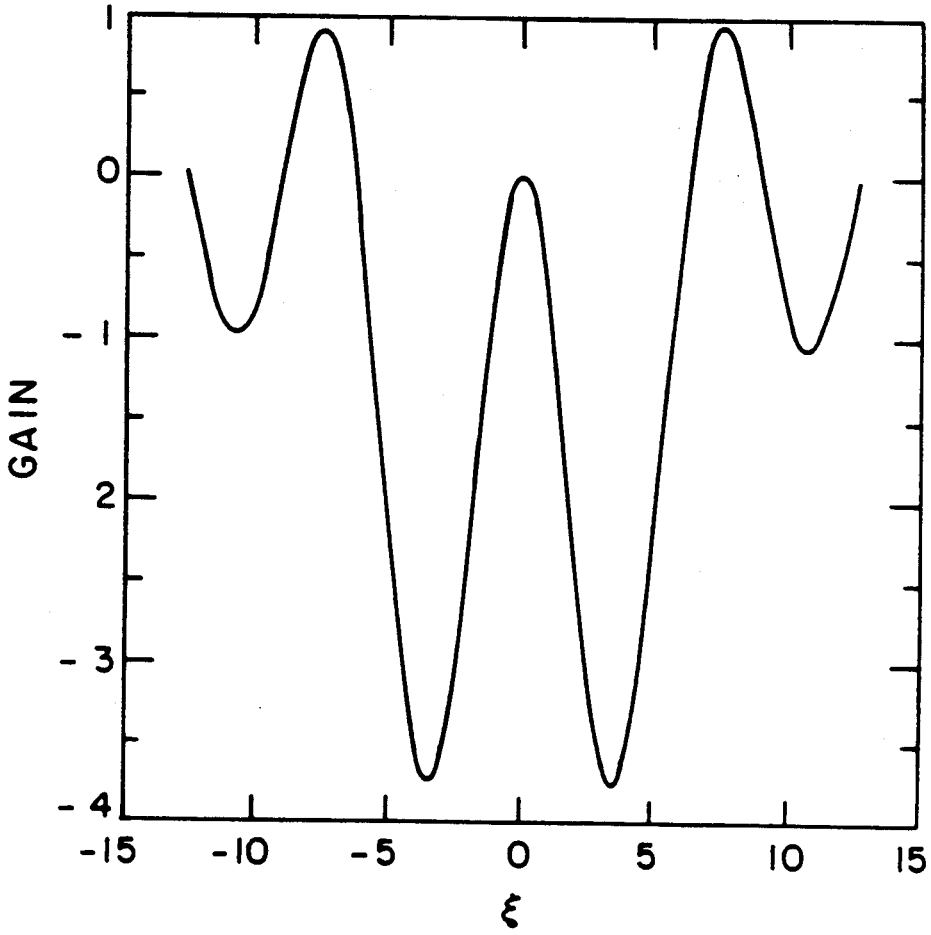


Fig. 1.b

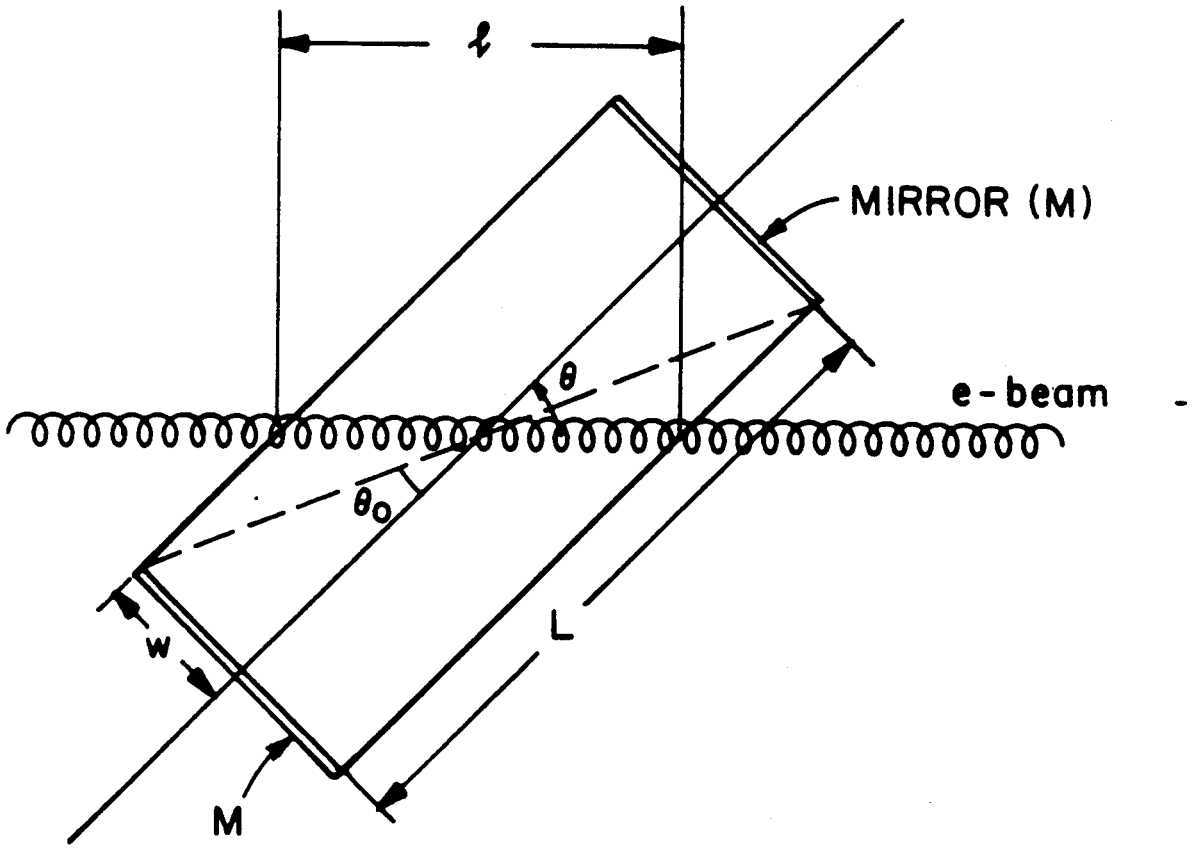


Fig. 2

Fig. 3.a

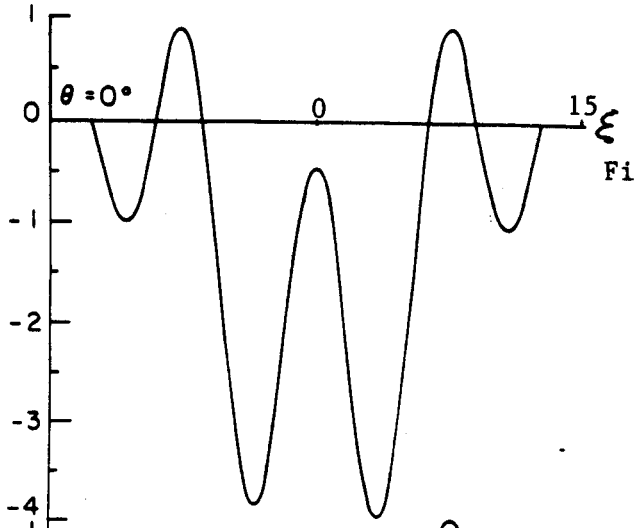


Fig. 3.b

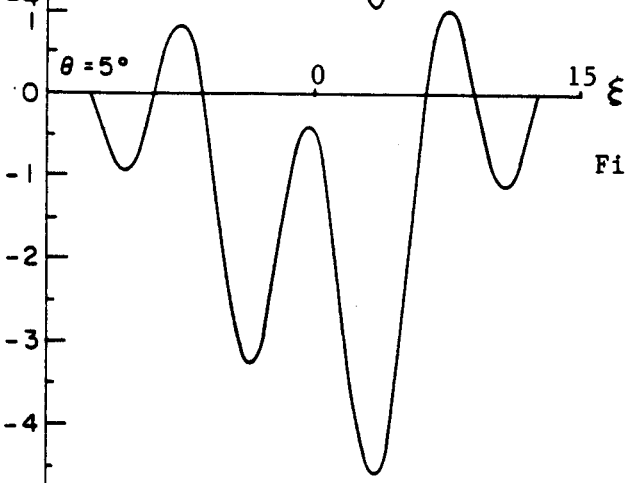


Fig. 3.c

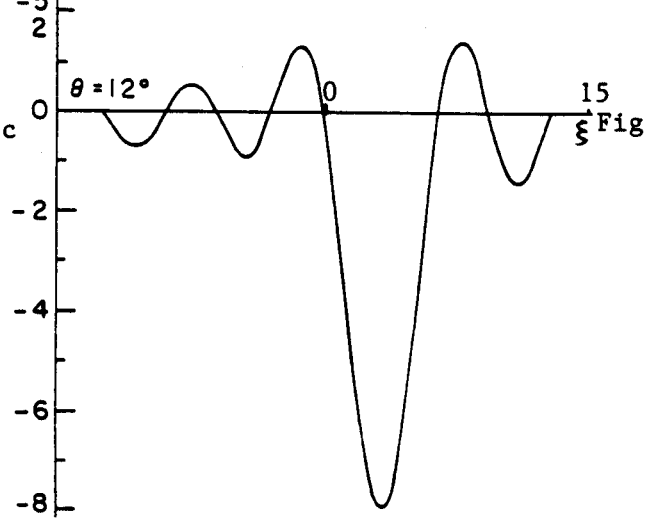


Fig. 3.d

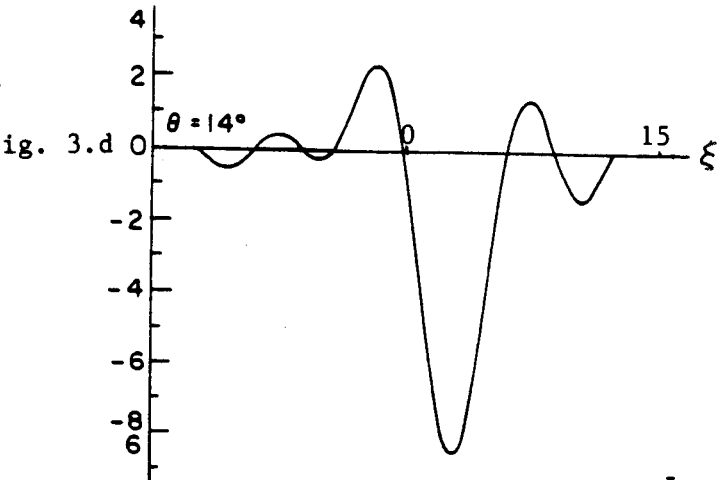


Fig. 3.e

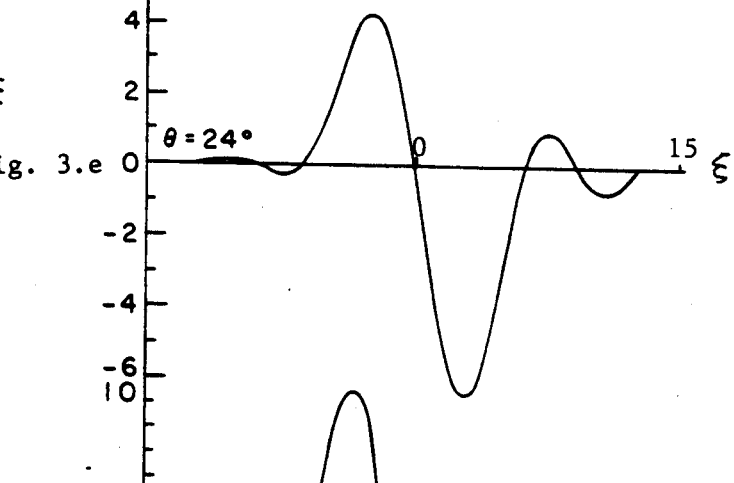


Fig. 3.f

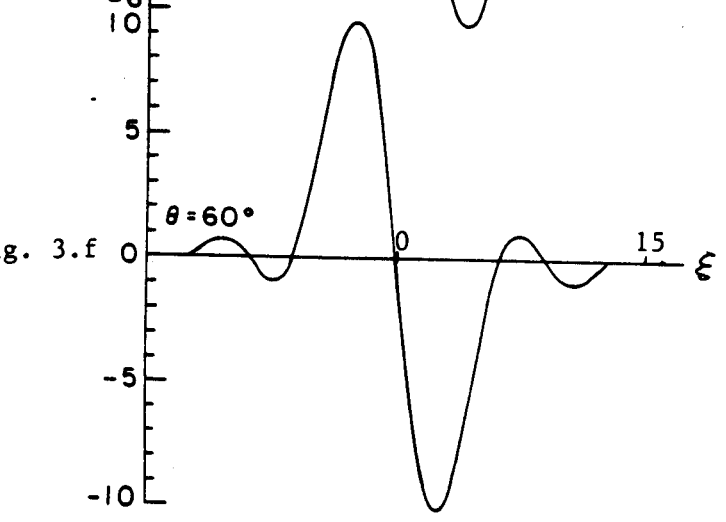

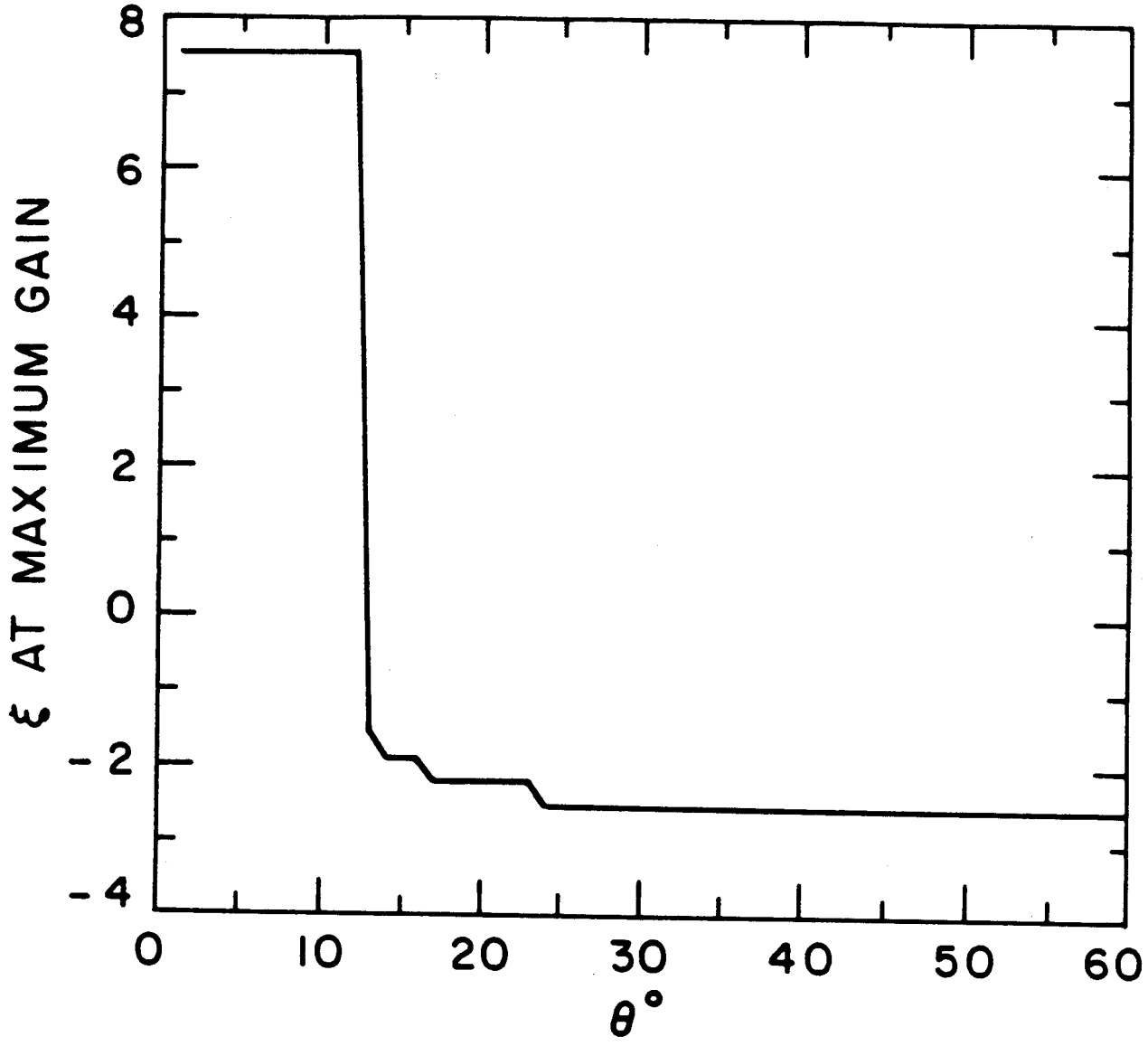


Fig. 4

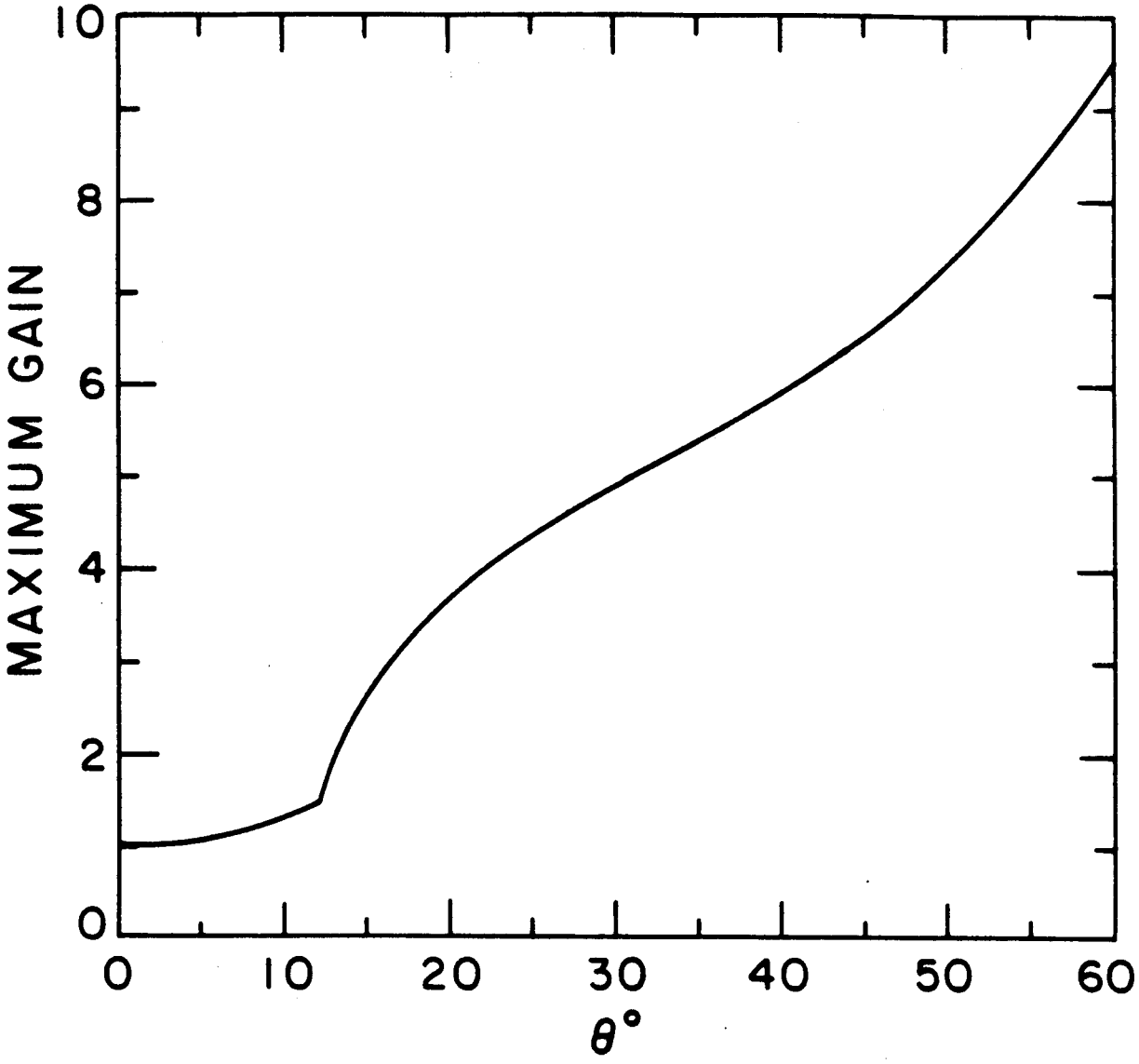


Fig. 5

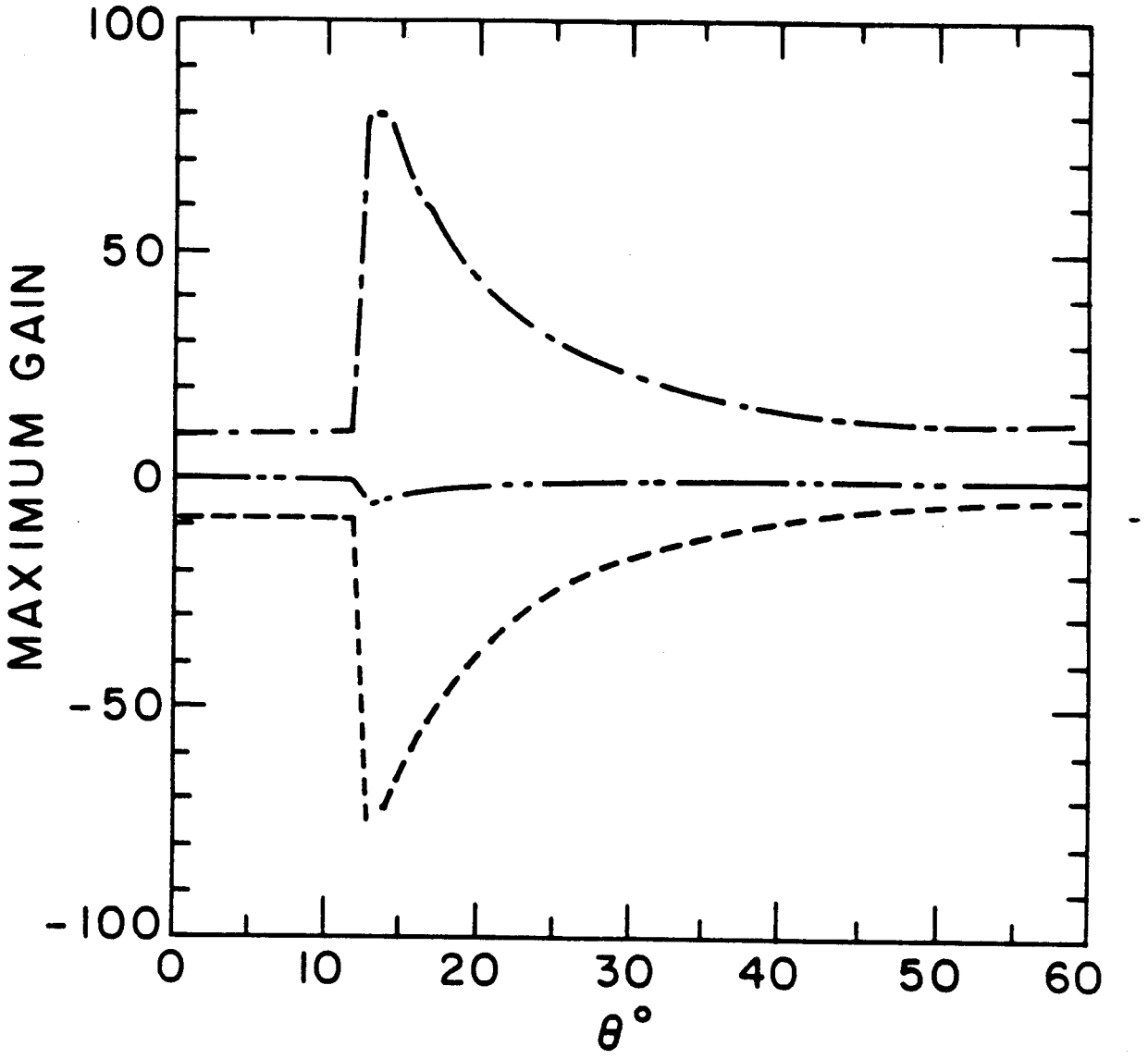


Fig. 6

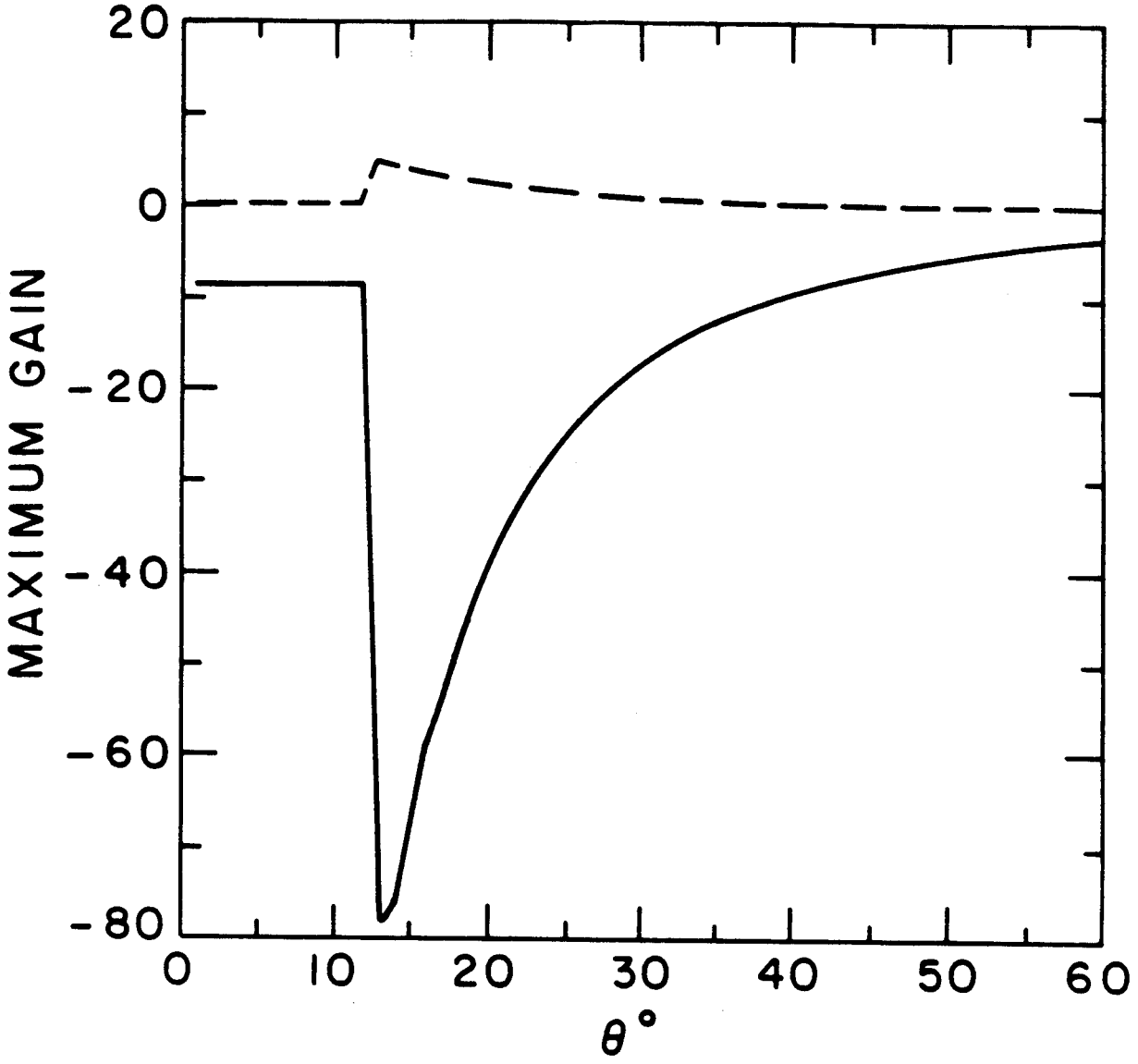


Fig. 7

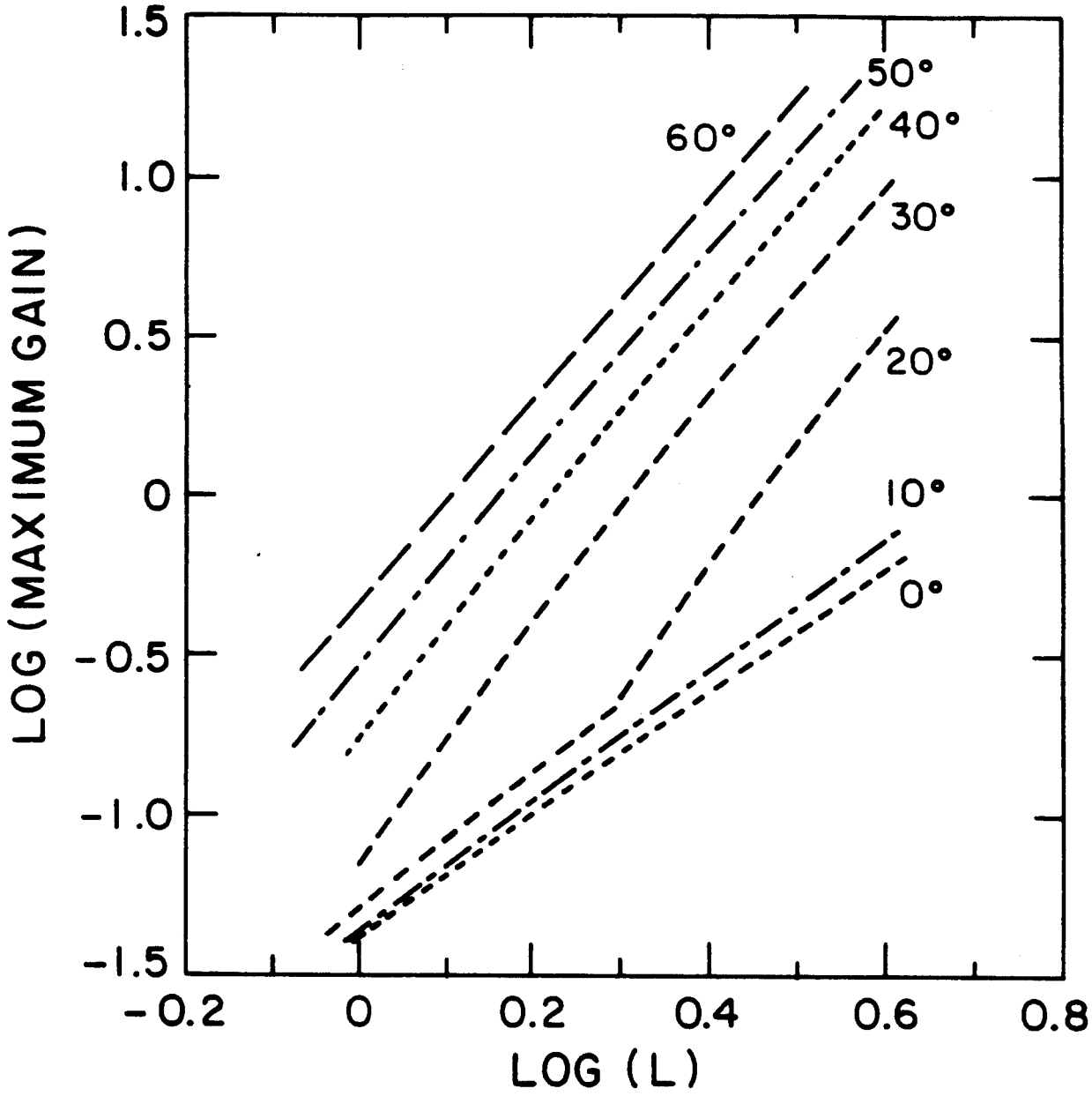
1.5
1.0
0.5
0
-0.5
-1.0
-1.5
-0.2
0
0.2
0.4
0.6
0.8
LOG (MAXIMUM GAIN)
LOG (L)
60°
50°
40°
30°
20°
10°
0°

Fig. 8

Fig. 9a

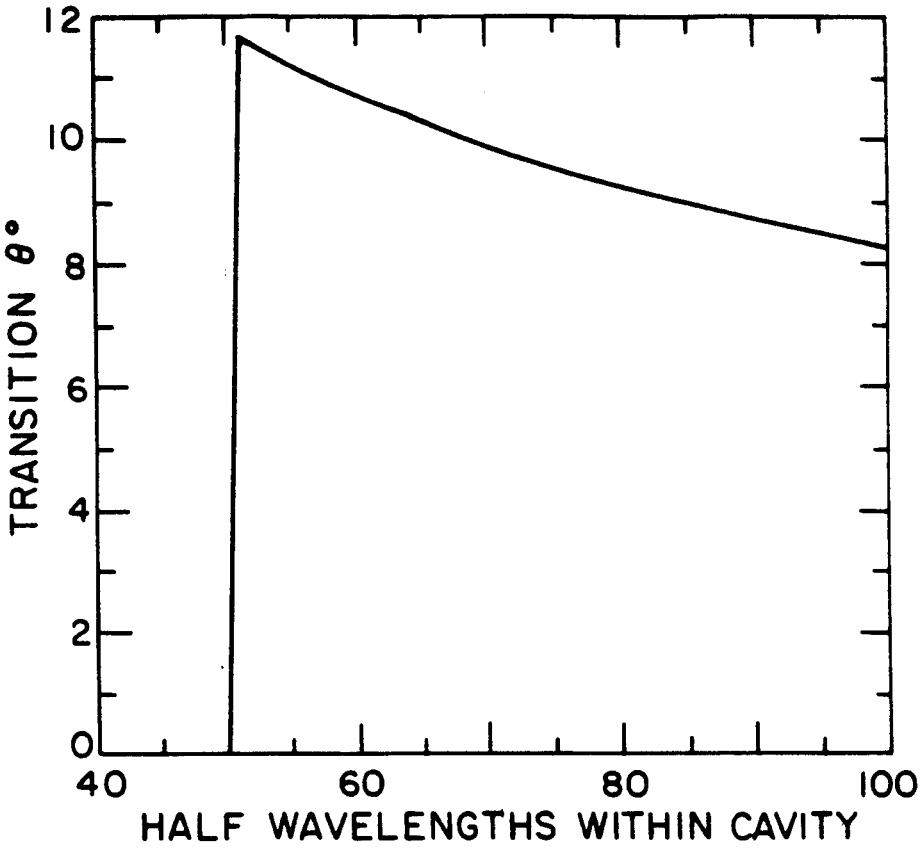
12
10
8
6
4
2
0
TRANSITION θ°
40
60
80
100
HALF WAVELENGTHS WITHIN CAVITY

Fig. 9b

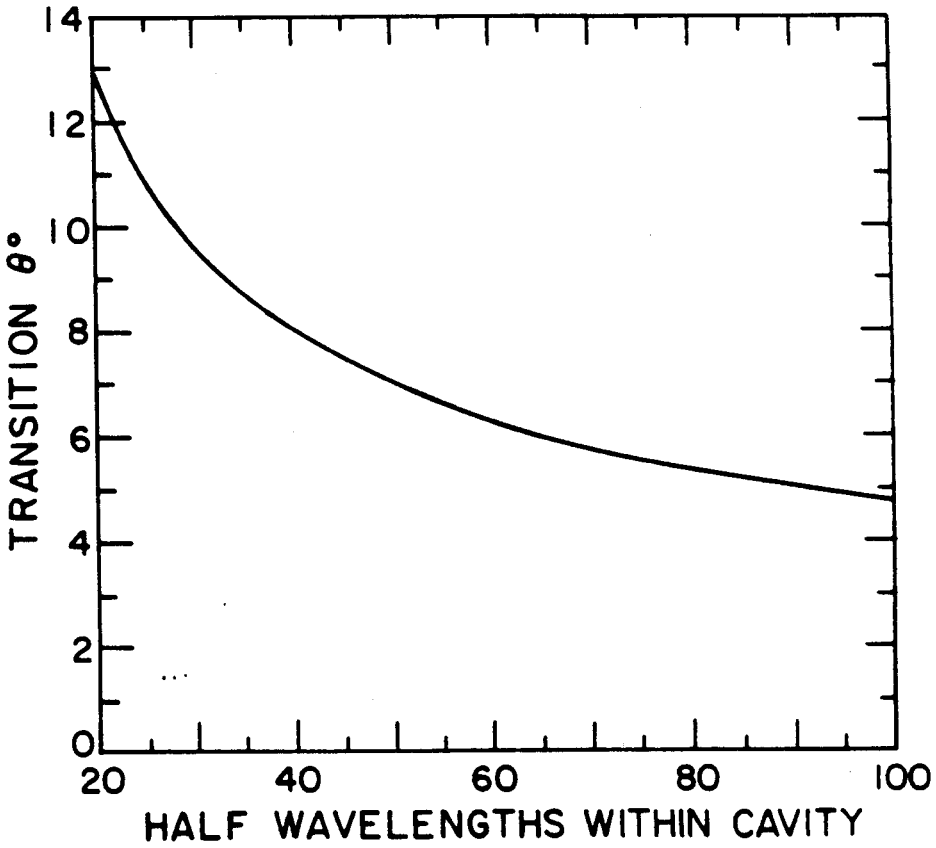
14
12
10
8
6
4
2
0
TRANSITION θ°
20
40
60
80
100
HALF WAVELENGTHS WITHIN CAVITY